Modeling of High-Voltage Induction Machines with Fallen-out Magnetic Slot Wedges

Milica Banović, Kristina Vujkov, *Student Member, IEEE*, Mladen Terzić, *Member, IEEE*, Dejan Jerkan, *Member, IEEE*

***Abstract*—Electrical machines of medium to high voltage range are commonly fabricated with wide stator slot openings which often lead to the increase of noise, vibrations and power losses. The use of magnetic slot wedges is intended to minimize these effects. Exposure to high magnetic and mechanical forces may cause magnetic wedge fall-outs. In this paper, a dynamical model of an induction machine was developed in order to investigate the influence of stator slot magnetic wedge failures on the machine's performance. Through observation of the machine's terminal quantity disturbances, the model demonstrated remarkable differences in steady-state rated operation, regarding stator line currents, rotor loop currents and generated electromagnetic toque, in case of healthy and faulty machine.**

***Index Terms*—induction machine; magnetic slot wedges; finite element analysis; MCCA; motor faults.**

I. Introduction

Induction machines (IMs) designed for use in modern drives and industry must cope with ever-growing demands for increased efficiency and high performance. Furthermore, there are strong requirements for the reduction of noise pollution and vibrations which represent one of the most common issues in today's motor drives. For high and medium voltage IMs, it is reported that wide open stator slots are the main cause of those issues [1-3]. A well-known means to mitigate suggested problems in medium and high voltage motors is to install magnetic stator slot wedges.

Most magnetic slot wedges are made from iron powder (~ 75%), glass fabric and epoxy resin binders, and therefore, have larger relative permeability (less than 10) compared to epoxy edges [4]. Their higher relative permeability compared to classical non-magnetic wedges reduces the flux fluctuations on the rotor core surface and decreases the effective air gap width. The smoothened flux [6] in the air gap reduces the surface core losses, acoustic noise and improves the torque characteristics [4, 5]. Therefore, magnetic slot wedges also improve motor efficiency, power factor and power density.

Since the iron powder in the magnetic wedges makes them mechanically weakened, they are more prone to failures (fall-outs) caused by exposure to high magnetic and mechanical forces. There are many cases of wedge failures in medium (high) voltage motors (above 3.3 kV) reported, where up to 50% of the wedges were lost within 3 years of service [4].

Magnetic wedge fall-outs impact the machine's performance and are observable through the IM terminal quantity disturbances. Numerical modeling of this phenomenon may be used as a starting point for the evaluation of this type of fault and investigation of reliable fault indicators.

For this purpose, a dynamical model of an IM, based on Multiple Coupled Circuit Approach (MCCA) and Finite Element Analysis (FEA) analysis [7-9] is developed in Section II. FEA calculations of IM inductances for the healthy and faulty machine are illustrated and discussed in Section III and then used for MCCA model inductance matrices formation. MCCA model simulation results, presented in Section IV clearly demonstrate the influence of magnetic slot wedge fall-outs through unbalanced stator line currents, distorted rotor bar currents and increased torque pulsation. Conclusion of this paper with further research topics suggestions is given in Section V.

II. Mathematical Representation of Mcca Model Of Squirrel-Cage Induction Motor

MCCA model of squirrel-cage IM is used to model energy conversion process in the machine, taking into account higher-order harmonic components in the magnetic field, induced voltages and currents. The nonsinusoidal electromagnetic field in the machine can be incorporated effectively by the rotor position-dependent variation of elements in MCCA model inductance matrices.

In this paper, the inductance matrix is reconstructed using series of linear 2-D FEA magneto-static simulations [7]. Discrete values of inductances obtained by this method are then represented via Fourier series, allowing the choice of harmonic components from the series which will be afterward used in the MCCA model.

The squirrel-cage rotor can be represented as identical and equally spaced rotor loops. Rotor loop consists of two neighboring rotors bars and adjacent end-ring segments. Fig. 1 shows three neighboring rotor loops (detail of rotor cage).

Milica Banović is with the School of Electrical Engineering, University of Belgrade, 73 Bulevar kralja Aleksandra, 11020 Belgrade, Serbia (e-mail: banovicmilicaa@gmail.com).

Kristina Vujkov is with the Faculty of Technical Sciences, University of Novi Sad, Trg Dositeja Obradovića 6, 21101 Novi Sad, Serbia (e-mail: kristina.vujkov@uns.ac.rs).

Dejan Jerkan is with the Faculty of Technical Sciences, University of Novi Sad, Trg Dositeja Obradovića 6, 21101 Novi Sad, Serbia (e-mail: dejan.jerkan@uns.ac.rs).

Mladen Terzić is with the School of Electrical Engineering, University of Belgrade, 73 Bulevar kralja Aleksandra, 11020 Belgrade, Serbia (e-mail: terzic@etf.bg.ac.rs).

 ISBN 978-86-7466-930-3

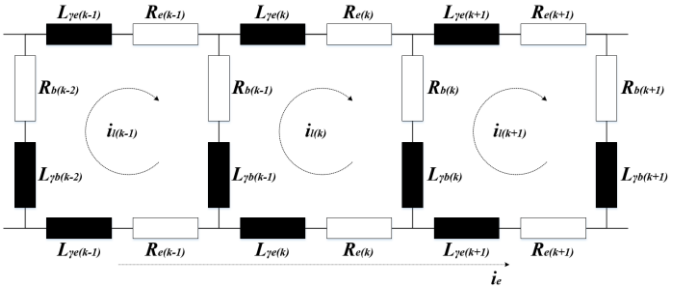

Fig. 1. Detail of squirrel-cage electrical circuit.

The mathematical model of the squirrel-cage IM can be formulated as:

$$\boldsymbol{V} = \boldsymbol{RI} + \frac{d}{dt}(\boldsymbol{LI}). \tag{1}$$

Voltage vector $\boldsymbol{V}$ consists of stator ($\boldsymbol{V_s}$) and rotor ($\boldsymbol{V_r}$) voltage vectors:

$$\begin{aligned} &\boldsymbol{V} = [\boldsymbol{V_s}\ \boldsymbol{V_r}]^T, \\ &\boldsymbol{V_s} = [v_a \quad v_b \quad v_c], \quad , \\ &\boldsymbol{V_r} = [0 \quad 0 \ldots 0 \quad 0]_{n_B+1.} \end{aligned} \tag{2}$$

where v_a, v_b, and v_c are three stator voltages and n_B is the number of rotor bars. There are $(n_B + 1)$ rotor voltages equal to zero for $(n_B + 1)$ independent current loops in the rotor cage which stand for n_B rotor bars and two end rings. Likewise voltage vector $\boldsymbol{V}$, current vector $\boldsymbol{I}$ in (1) consists of stator ($\boldsymbol{I_s}$) and rotor ($\boldsymbol{I_r}$) current vectors:

$$\begin{aligned} &\boldsymbol{I} = [\boldsymbol{I_s}\ \boldsymbol{I_r}]^T, \\ &\boldsymbol{I_s} = [i_a \quad i_b \quad i_c], \quad . \\ &\boldsymbol{I_r} = [i_{l1} \quad i_{l2} \ldots i_{ln_B} \quad i_e]_{n_B+1,} \end{aligned} \tag{3}$$

where $\boldsymbol{I_s}$ is the stator current vector for three stator phase windings i_a, i_b, and i_c. Rotor current vector $\boldsymbol{I_r}$ includes n_B rotor loops currents i_{r1}, i_{l2}, …, i_{ln_B} and one end-ring current i_e.

Diagonal 3x3 stator resistance matrix $\boldsymbol{R_s}$ and rotor resistance symmetrical matrix $\boldsymbol{R_r}$ comprise resistance matrix $\boldsymbol{R}$ from (1):

$$\begin{aligned} &\boldsymbol{R} = \begin{bmatrix} \boldsymbol{R_s} & \\ & \boldsymbol{R_r} \end{bmatrix}, \\ &\boldsymbol{R_s} = \begin{bmatrix} R_s & & \\ & R_s & \\ & & R_s \end{bmatrix}, \\ &\boldsymbol{R_r} = \begin{bmatrix} R_{l1} & -R_{b2} & \ldots & -R_{bn_B} & -R_{e1} \\ -R_{b1} & R_{l2} & \ldots & 0 & -R_{e2} \\ \vdots & \vdots & \ldots & \vdots & \vdots \\ \vdots & \vdots & \ldots & \vdots & \vdots \\ 0 & 0 & \ldots & -R_{bn_B} & -R_{e(n_B-1)} \\ -R_{b1} & 0 & \ldots & R_{ln_B} & -R_{en_B} \\ -R_{e1} & -R_{e2} & \ldots & -R_{en_B} & \sum_{i=1}^{N_B} R_{ei} \end{bmatrix}_{(n_B+1)\mathrm{x}(n_B+1)} \end{aligned} \quad , \tag{4}$$

where R_{lk} represents resistance of rotor k loop, defined as $R_{lk} = R_{bk} + R_{b(k+1)} + 2R_{ek}$ with R_{bk} as k bar resistance and R_{ek} end-ring k segment resistance.

Interaction between neighboring rotor loops and end-ring segments shown in Fig. 1 are reflected in the resistance matrix $\boldsymbol{R_r}$. Voltage equation for arbitrarily k rotor loop ($1 < k \leq N_B$) (Fig. 1) has the following form:

$$\begin{aligned} R_{ek} i_{rlk} + R_{bk}\left(i_{rlk} - i_{rl(k+1)}\right) + R_{ek}(i_{rlk} - i_e) - \\ R_{b(k-1)}\left(i_{rl(k-1)} - i_{rlk}\right) + \frac{d\Psi_{\mathrm{rlk}}}{dt} = 0, \end{aligned} \tag{5}$$

It can be noticed that negative elements in the matrix $\boldsymbol{R_r}$ (4) result from interactions between neighboring rotor loops and end ring.

Rotor bar current i_{bk} can be expressed through neighboring rotor loop currents as follows:

$$i_{bk} = i_{lk} - i_{l(k+1)}. \tag{7}$$

Inductance matrix $\boldsymbol{L}$ is a periodic function of rotor angular position θ, and it consists of four sub-matrices:

$$\boldsymbol{L}(\theta) = \begin{bmatrix} \boldsymbol{L_{ss}}(\theta) & \boldsymbol{L_{sr}}(\theta) \\ \boldsymbol{L_{rs}}(\theta) & \boldsymbol{L_{rr}}(\theta) \end{bmatrix}. \tag{8}$$

Stator inductance matrix $\boldsymbol{L_{ss}}$ is θ-dependent 3x3 matrix which defines magnetic coupling between stator phases:

$$\boldsymbol{L_{ss}}(\theta) = \begin{bmatrix} L_a & M_{ab} & M_{ac} \\ M_{ba} & L_b & M_{bc} \\ M_{ca} & M_{cb} & L_c \end{bmatrix}. \tag{9}$$

Rotor inductance matrix $\boldsymbol{L_{rr}}$ is a $(n_B + 1)$x$(n_B + 1)$ position-varying matrix generated similarly to rotor resistance matrix with one major difference; any rotor loop is magnetically coupled with all the other loops and generally there are no zero elements in it:

$$\boldsymbol{L_{rr}}(\theta) = \begin{bmatrix} L_{l1} & \ldots & M_{r1n_B} - L_{bn_B} & -L_{\gamma e1} \\ M_{r21} - L_{b1} & \ldots & M_{r2n_B} & -L_{\gamma e2} \\ \vdots & \ldots & \vdots & \vdots \\ \vdots & \ldots & \vdots & \vdots \\ M_{r(n_B-1)1} & \ldots & M_{r(n_B-1)n_B} - L_{bn_B} & -L_{\gamma e(n_B-1)} \\ M_{rn_B1} - L_{b1} & \ldots & L_{ln_B} & -L_{en_B} \\ -L_{e1} & \ldots & -L_{en_B} & \sum_{i=1}^{n_B} L_{ei} \end{bmatrix}. \tag{10}$$

Rotor k loop inductance L_{lk} ($1 \leq k \leq n_B$) is defined as $L_{lk} = L_k + L_{\gamma bk} + L_{\gamma b(k+1)} + 2L_{\gamma ek}$, where L_k is k loop self-inductance, $L_{\gamma bk}$ is rotor k bar leakage inductance, and $L_{\gamma ek}$ is rotor end-ring k segment leakage inductance. Mutual inductances between arbitrary rotor loops m and n are labeled as M_{rmn} ($1 \leq m, n \leq n_B \wedge m \neq n$).

Stator-rotor inductance matrix $\boldsymbol{L_{sr}}$ is defined as:

 ISBN 978-86-7466-930-3

$$\boldsymbol{L_{sr}}(\theta) = \begin{bmatrix} M_{al1} & M_{al2} & \dots & M_{al_{n_B}} & 0 \\ M_{bl1} & M_{bl2} & \dots & M_{bl_{n_B}} & 0 \\ M_{cl1} & M_{cl2} & \dots & M_{cl_{n_B}} & 0 \end{bmatrix}, \quad (11)$$

Mutual inductance between arbitrarily stator phase x and rotor loop k is labeled as M_{xlk}, where $x \in \{a, b, c\}, 1 \leq k \leq n_B$. Rotor-stator inductance matrix $\boldsymbol{L_{rs}}$ can be derived from (11), by transposition of stator-rotor inductance matrix $\boldsymbol{L_{rs}} = \boldsymbol{L_{sr}^T}$.

The calculation of torque T_e in the MCCA model is based on the virtual work principle (p is pole pairs number):

$$T_e = \frac{1}{2} p \begin{bmatrix} \boldsymbol{I_s} \\ \boldsymbol{I_r} \end{bmatrix}^T \frac{d}{d\theta} \left(\begin{bmatrix} \boldsymbol{L_{ss}} & \boldsymbol{L_{sr}} \\ \boldsymbol{L_{rs}} & \boldsymbol{L_{rr}} \end{bmatrix} \right) \begin{bmatrix} \boldsymbol{I_s} \\ \boldsymbol{I_r} \end{bmatrix}. \quad (12)$$

III. Inductance Calculation of Healthy and Faulty IM

After derivation of MCCA model in Section II, inductance calculation method shall be presented in the following. Modeled induction machine is a 2-pole, 6 kV high voltage motor with rated output power of 1.03 MW (detailed machine data are given in Appendix). Magnetic slot wedges of relative permeability 5 are used to close stator slot openings.

Linear magneto-static 2-D FEA simulations are used to compute discrete values of machine's inductances relative to absolute rotor angular position. Saturation effect is neglected. In the calculated inductance waveforms, only harmonics provoked by geometry variations and presence/absence of the magnetic wedges are investigated. These harmonics are independent from saturation-induced harmonics and can be treated separately.

In order to obtain self- and mutual inductances of an arbitrary winding for a fixed rotor position, only the winding itself is supplied with 1 A direct current. After single magneto-static simulation is completed, flux linkages of all windings in the machine are determined and used for single discrete value inductance calculation. Next magneto-static simulation is performed in the same manner after fixed-valued angle increment of rotor position. The value of angle increment determines the precision of inductances waveforms.

One full revolution of rotor is necessary for complete inductance matric reconstruction. Derived discrete waveforms are then represented with Fourier series coefficients in the MATLAB&Simulink model.

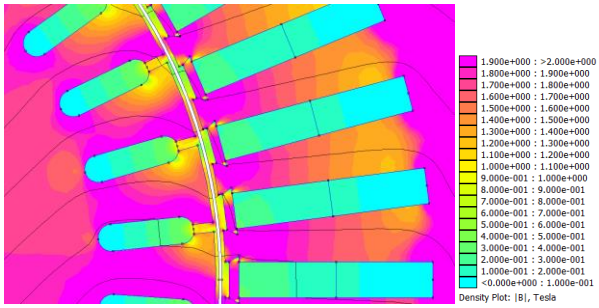

Fig. 2. Discrete magneto-static simulation of healthy IM

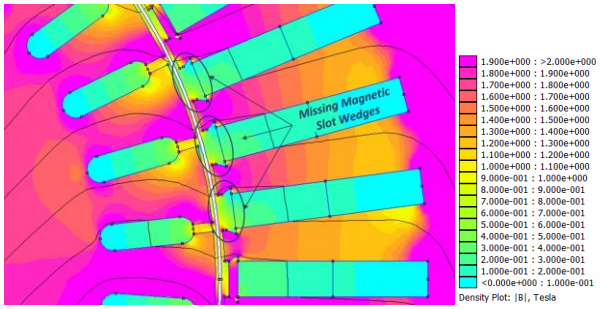

Fig. 3. Discrete magneto-static simulation of faulty IM (three consecutive fallen-out wedges)

Detail of magneto-static simulation for healthy and faulty IM is given in Fig. 2 and Fig. 3, respectively. The analyzed fault is modeled by three consecutive completely fallen-out wedges. As can be seen from the figures magnetic flux lines crossing the air gap from rotor to stator have significantly more homogeneous flow in the healthy motor compared to the one with missing wedges. Represented local distortion of flux lines will lead to deformation of machine inductances in case of fault occurrence.

Stator phase *A* self-inductance as a function of rotor angular position is shown in Fig. 4. Minor oscillations around the constant value of stator self-inductance are the result of air gap equivalent permeability variations caused by rotor slotting. Since analyzed IM has 36 rotor slots all three stator self-inductances have identical waveforms and their minor oscillations are in phase.

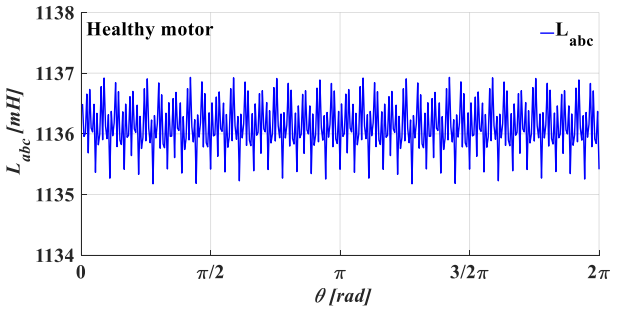

Fig. 4. Stator phase A self-inductance waveform – healthy motor

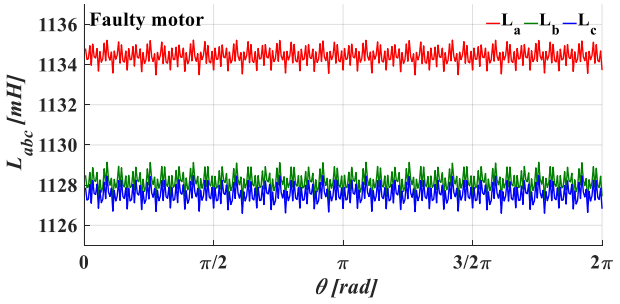

Fig. 5. Stator phases self-inductances waveform – faulty motor

In case of fallen-out wedges, the balance of stator

 ISBN 978-86-7466-930-3

windings is corrupted. This leads to different mean values of stator self inductances for phase *A*, *B*, and *C*. Modeled missing wedges are in close vicinity of phase *B* and *C* winding axes. Lack of ferromagnetic material caused by fallen-out magnetic wedges decreases inductances of most affected windings - Fig. 5.

Similar phenomena can be observed in stator mutual inductance waveforms. All stator mutual inductances are identical in case of healthy motor (Fig. 6), while in the event of fault (Fig. 7), all mutual inductances suffer in mean value reduction. Mutual inductances involving phase *A* are less influenced by the fault, as expected.

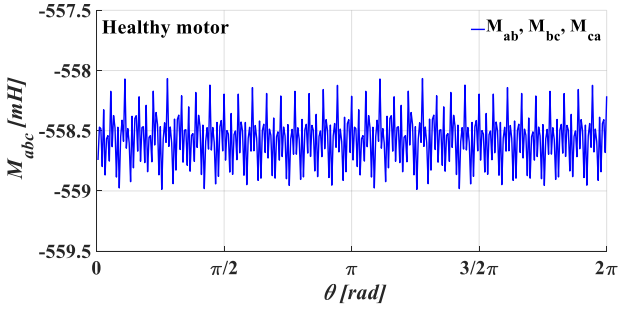

Fig. 6. Stator phases mutual inductances waveform – healthy motor

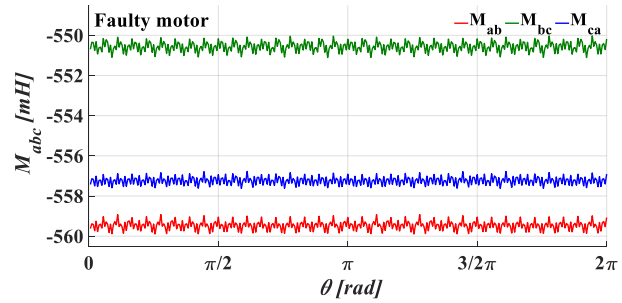

Fig. 7. Stator phases mutual inductances waveform – faulty motor

Stator-rotor inductances of IM are the main contributors to torque generation. For healthy motor, they are symmetrical, alternating, rotor angular position-dependent functions with characteristic trapezoidal shape (Fig. 8 – blue line). Therefore, spectrum of trapezoidal inductance signal contains only odd higher-order harmonics (Fig. 9 – blue bars). However, in the presence of slot wedge faults, a local dip in the waveform is formed each time specific rotor loop passes by stator slots with missing wedges (Fig. 8 – red line). As a result, new even harmonic components in the Fourier series appear (Fig. 9 – red bars). These additional components will further induce characteristic harmonics in flux linkages and consequently, in induced voltages and currents. This will affect torque production by causing unwanted pulsations.

The fallen-out magnetic slot wedges also have impact on rotor inductance matrix. Similar to stator inductances, rotor inductances in the healthy machine are fairly constant quantities with small oscillations around the mean value. These oscillations are the consequences of stator slotting. Slot wedges reduce these oscillations by making stator inner circumference more magnetically uniformed.

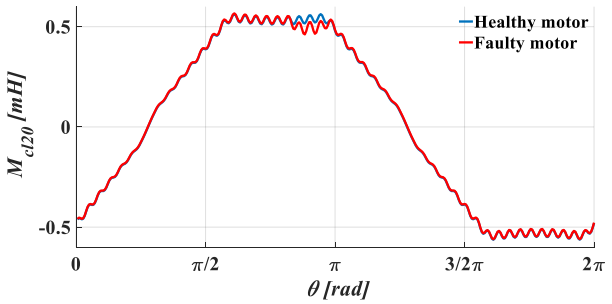

Fig. 8. Mutual inductance between stator phase C and rotor loop 20

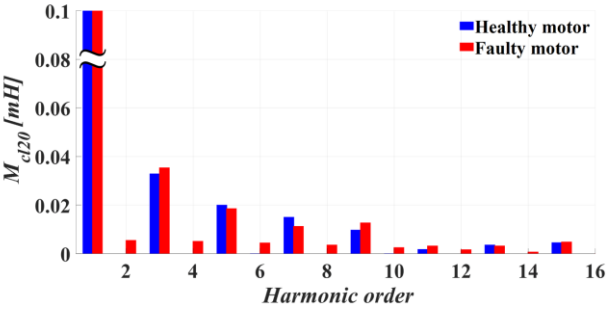

Fig. 9. Mutual inductance between stator phase C and rotor loop 20 - Fourier series coefficients

In Fig. 10 blue line illustrates rotor loop self-inductance waveform in healthy motor. There are exactly 48 oscillations in one rotor revolution due to the number of stator slots. When slot wedges are missing stator magnetic uniformity is lost which will locally diminish rotor self-inductance just as rotor loop passes by faulty slots. Since three neighboring slots are impacted by the fault, there will be three more prominent oscillations combined with lower mean value in the inductance waveform (Fig. 10 – red line).

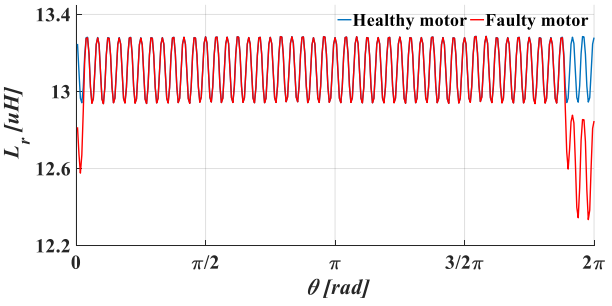

Fig. 10. Rotor loop self-inductance

A detail of rotor self-inductance spectrum, both for healthy and faulty motor, is shown in Fig. 11. In order to emphasize the emergence of additional spectral components, dominant mean value is excluded from the figure. Despite their small magnitudes, higher-order components have a significant impact on the energy conversion process which will be

 ISBN 978-86-7466-930-3

illustrated and discussed in the next Section.

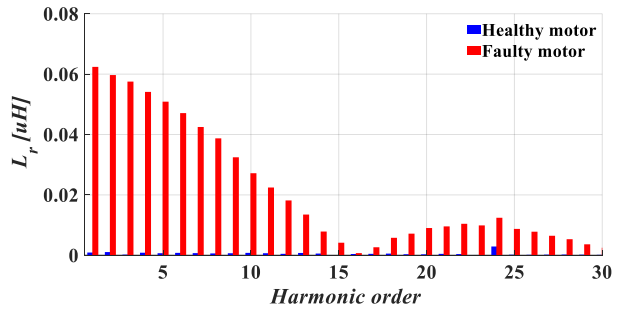

Fig. 11. Rotor loop self-inductance – spectrum with mean value excluded

As the last characteristic example of the magnetic wedge fall-outs impact on machine's inductances, mutual inductance between arbitrarily chosen rotor loops is shown in Fig. 11 (healthy machine in blue and faulty in red line). Magnetic coupling between two rotor loops subjects to complex mechanisms of flux lines formation and it is dependent on relative rotor position and the mutual position of the loops themselves. The situation grows even more puzzling when slot wedge fault is present, as observable in Fig. 11- red line.

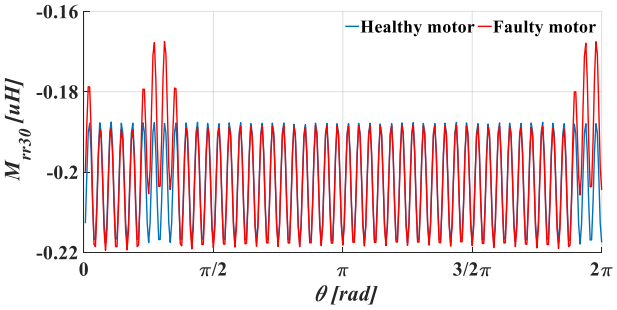

Fig. 12. Mutual inductance between first and 31st rotor loop

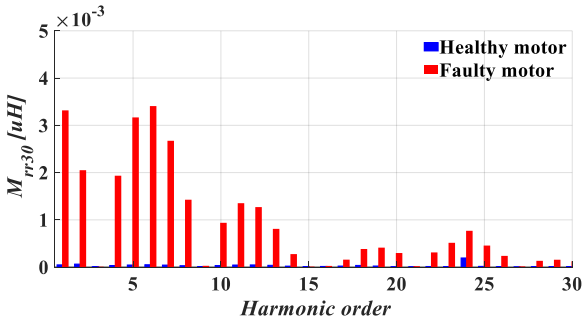

Fig. 13. Mutual inductance between first and 31st rotor loop – spectrum with mean value excluded

Singled out higher-order components of the mutual inductance between first and 31st rotor loop, shown in Fig. 13 are compliant with the expected increase in number and magnitude of additional components in the spectrum, similar to elaborated phenomena in Fig. 11.

IV. Simulation Results

Based on FEA calculation of machine's inductances presented in Section III and MCCA model derived in Section II MATLAB&Simulink model of the machine under investigation (Appendix) was developed.

The output of FEA computations i.e. waveforms of machine inductances are firstly represented with Fourier series coefficients. These coefficients are then used for the formation of time and position varying inductance matrices of dynamic MCCA machine model. Inductances independent from geometry variations which cannot be calculated using 2-D representation of the machine: stator end-winding and rotor end-ring leakage inductances are added to the MCCA model inductance matrices as constant values. Their values are provided from separate simulations performed using commercial FEA software with such built-in options. MCCA model is able to simulate transient behavior of the machine under arbitrary supply and loading conditions, similar to conventional dq models, but with much more insight into construction-dependent properties of the specific machine.

Stator line currents during steady-state operation under the rated load of healthy machine are illustrated in Fig. 14. The machine was supplied from three-phase balanced voltage source of 6 kV at rated frequency of 50 Hz. Rated speed of the machine was 2985 rpm, rated torque 3.23 kNm and rated output power 1.03 MW. As expected, line currents are balanced in the case of healthy machine.

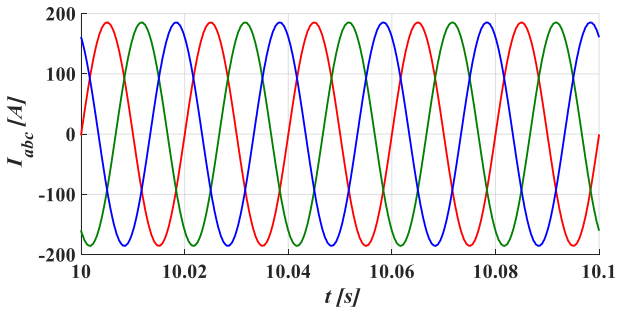

Fig. 14. Stator line currents under full load – healthy machine

Under the same supply and loading conditions, but with magnetic wedge fault present, unbalance in stator line currents is clearly visible in Fig. 15. Fallen-out magnetic wedges led to unbalanced inductances of stator phase windings (Fig. 5 and 7) which consequently caused noticeable imbalance in the currents as well.

Fig. 16 shows differences between arbitrary rotor loop current waveforms in case of the healthy and faulty machine. It is noticeable that, in the event of fault, rotor loop current waveform will contain more prominent oscillations which were expected as the result of emergence of additional components in the inductance spectrum of the faulty machine.

 ISBN 978-86-7466-930-3

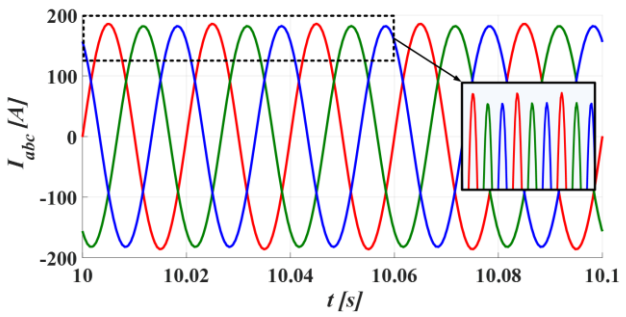

Fig. 15. Stator line currents under full load – faulty machine

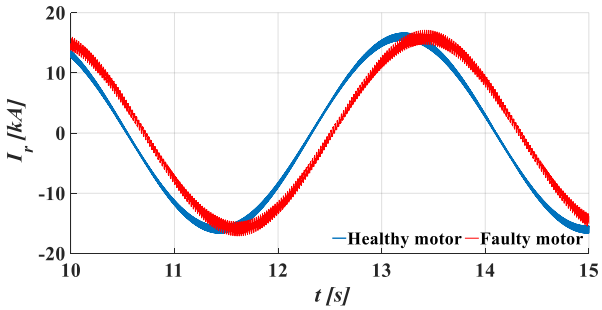

Fig. 16. Current waveform of arbitrary rotor loop under full load

Parasitic torque pulsations are direct outcome of increased oscillations in the machine inductances and currents. In the Fig. 17, the machine toque waveform is illustrated for rated operational mode with and without fault. Increased torque pulsations may provoke an unwanted mechanical response from the machine which could reflect on the level of noise and vibrations. Exceeding level of vibration can have great impact on bearing deterioration, may cause cracks in the winding insulation and tightness of the lamination stack.

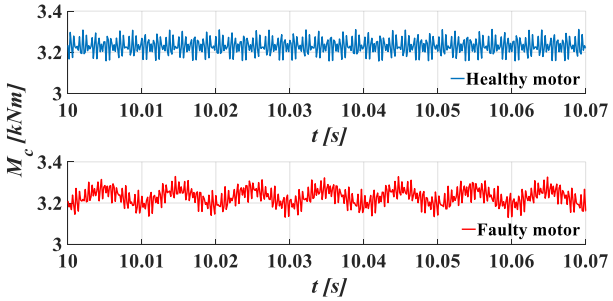

Fig. 17. Rated electromagnetic torque

V. Conclusion

In this paper MCCA model of high voltage squirrel-cage induction machine is used to investigate the influence of stator slot magnetic wedge failures on machine's performance. Series of magneto-static FEA simulations illustrated differences in waveforms of characteristic inductances of the machine in case of healthy machine and the machine with three consecutive fallen-out stator magnetic wedges. FEA results provided input data for MCCA inductance matrices formation, using the Fourier series coefficient. Through observation of the machine's terminal quantity disturbances, performed simulations in MATLAB&Simulink dynamic MCCA model of IM demonstrated remarkable differences in steady-state rated operation, regarding stator line currents, rotor loop currents and generated electromagnetic toque. Further research may include targeted thorough analysis of the terminal quantities in the interest of reliable and non-invasive detection of fallen-out wedges.

Appendix

TABLE I
Motor Parameters

Rated Power	*1.03 MW*
Rated Speed	*2985 rpm*
Rated Torque	*3.23 kNm*
Rated Voltage	*6 kV*
Number of Stator Slots	*48*
Number of Rotor Slots	*36*
Stator Inner/Outer Diameter	*430/780 mm*
Air Gap Width	*4 mm*
Lamination Stack Length	*765 mm*

References

[1] G. Stojicic, M. Vasak, N. Peric, G. Joksimovic and T. M. Wolbank, "Detection of partially fallen-out magnetic slot wedges in inverter fed AC machines under various load conditions," 2012 IEEE Energy Conversion Congress and Exposition (ECCE), 2012, pp. 4015-4020.

[2] G. Stojičić et al., "A method to detect missing magnetic slot wedges in AC machines without disassembling," IECON 2011 - 37th Annual Conference of the IEEE Industrial Electronics Society, 2011, pp. 1698-1703.

[3] G. Stojicic, M. Vasak, N. Peric, G. Joksimovic and T. M. Wolbank, "Detection of partially fallen-out magnetic slot wedges in inverter fed AC machines under various load conditions," 2012 IEEE Energy Conversion Congress and Exposition (ECCE), 2012, pp. 4015-4020.

[4] K. W. Lee et al., "Detection of Stator-Slot Magnetic Wedge Failures for Induction Motors Without Disassembly," in IEEE Trans. on Industry Applications, vol. 50, no. 4, pp. 2410-2419, July-Aug. 2014.

[5] Shuping Wang, Zhengming Zhao, Liqiang Yuan and Buyao Wang, "Investigation and analysis of the influence of magnetic wedges on high voltage motors performance," 2008 IEEE Vehicle Power and Propulsion Conference, 2008, pp. 1-6.

[6] H. Mikami, K. Ide, K. Arai, M. Takahashi and K. Kajiwara, "Dynamic harmonic field analysis of a cage type induction motor when magnetic slot wedges are applied," in IEEE Trans. on Energy Conversion, vol. 12, no. 4, pp. 337-343, Dec. 1997.

[7] D. G. Jerkan, D. D. Reljić and D. P. Marčetić, "Broken Rotor Bar Fault Detection of IM Based on the Counter-Current Braking Method," in IEEE Trans. on Energy Conversion, vol. 32, no. 4, pp. 1356-1366, Dec. 2017.

[8] Xiaogang Luo, Yuefeng Liao, H. A. Toliyat, A. El-Antably and T. A. Lipo, "Multiple coupled circuit modeling of induction machines," in IEEE Trans. on Industry Applications, vol. 31, no. 2, pp. 311-318, March-April 1995.

[9] M. Ojaghi, M. Sabouri and J. Faiz, "Performance Analysis of Squirrel-Cage Induction Motors Under Broken Rotor Bar and Stator Inter-Turn Fault Conditions Using Analytical Modeling," in IEEE Trans. on Magnetics, vol. 54, no. 11, pp. 1-5, Nov. 2018, Art no. 8203705.

 ISBN 978-86-7466-930-3